

A variational model with hybrid Hyper-Laplacian priors for Retinex



Ming-Hui Cheng^a, Ting-Zhu Huang^{a,*}, Xi-Le Zhao^{a,*}, Tian-Hui Ma^b, Jie Huang^a

^aSchool of Mathematical Sciences, University of Electronic Science and Technology of China, Chengdu, Sichuan 611731, PR China

^bSchool of Mathematics and Statistics, Xi'an Jiaotong University, Xi'an 710049, PR China

ARTICLE INFO

Article history:

Received 17 October 2017

Revised 4 August 2018

Accepted 18 September 2018

Available online 21 September 2018

Keywords:

Retinex

Illumination

Reflection

Hyper-Laplacian

Alternating direction method of multipliers

ABSTRACT

Retinex aims at estimating real reflectance images by removing the effect of illumination. We propose a nonconvex variational model for Retinex with novel priors for reflectance and illumination. Based on the statistics of the gradients of reflectance and illumination, we use the hyper-Laplacian prior to characterize the gradients of reflectance, and the hybrid hyper-Laplacian and Tikhonov prior to characterize the gradients of illumination. An efficient alternating direction method of multipliers (ADMM) is developed to solve the proposed model. Extensive numerical experiments show that the proposed method is comparable to the state-of-the-art methods quantitatively and qualitatively.

© 2018 Elsevier Inc. All rights reserved.

1. Introduction

Land and McCann [1] first proposed the idea of Retinex to explain the human visual system, where the colors of objects remain constant under different illumination situations. The objective of Retinex is to get rid of the non-uniform illumination effect in order to recover the original colors and details of an image.

In the Retinex theory, an observed image S is modeled as

$$S = L \circ R, \quad (1)$$

where \circ denotes the point-wise multiplication. Here R is the reflectance component in the range $(0,1]$, where the boundaries zero and one mean total absorption and total reflection, respectively; L is the illumination component in the range $(0, \infty)$. It is clear that $0 < S \leq L$. Specifically, the reflectance should contain only details without light intensity; the illumination should only contain light intensity with as less details as possible.

There are many methods for Retinex. Early contributions are path-based [1–6] and PDE-based [7–10]. Path-based methods need to adjust many parameters and cost too much time to get the results. PDE-based models decompose the observed images into reflectance and illumination according to the physical information. Recently proposed methods are variational-based. They formulate the Retinex problem as an optimization problem, where reflectance and illumination are characterized by some priors. Common priors for reflectance include total variation (TV) [11–14], nonlocal TV [15,16], L_1 -based priors [17], adaptive priors [18], and sparsity under a learned dictionary [19]. Common priors for illumination include Tikhonov

* Corresponding authors.

E-mail addresses: mhcheng10631@163.com (M.-H. Cheng), tzhuang@uestc.edu.cn (T.-Z. Huang), xlzhao122003@163.com (X.-L. Zhao), nkmth0307@126.com (T.-H. Ma), happyjie07mo@163.com (J. Huang).

regularization [12–14,20], nonlocal TV [15,16], and high order TV [21]. However, those common priors for reflectance and illumination have their drawbacks. The reflectance is sparse on gradients due to the fact that there is a low number of albedos in an image in the Retinex theory. TV and $L1$ -based methods usually lead to suboptimal results [22], since they are not good approximations of the sparsity. On the other hand, methods that utilize the smoothness prior for illumination [12–14,20] can not preserve details while preventing overexposure. Although the global smoothness prior can describe the varieties of light intensity and estimate details, it is difficult to distinguish the edges of different lightness regions.

An effective tool to overcome the above drawbacks is the analyzing of the statistics of natural images, which gets remarkable progress in image processing. Huang and Mumford [23] introduced the scale invariant property of natural images, and used the Ising-like MRF for natural images simulation. Then, Ruderman [24] proposed a new symmetry named variance normalization. Besides the above statistics of images, the heavy-tailed distribution of natural images is common and significant in the gradient domain and can be well fitted by the hyper-Laplacian [25–28]. The hyper-Laplacian distribution can be written as

$$p(x) \propto e^{-k|x|^\alpha}, \quad (2)$$

where α , k are parameters and $0 < \alpha < 1$. In sparse coding, it is known as l_p -seminorm ($0 < p < 1$), i.e., $\lambda \|x\|_p^p$. In 2009, Krishnan and Fergus [28] applied the hyper-Laplacian prior to non-blind deconvolution and proposed a fast algorithm to solve their model. Later, Zuo et al. [29] introduced the hyper-Laplacain prior to model the image gradients for blind deconvolution and proposed a principled discriminative learning model to handle the parameter tuning. Chang et al. [30] utilized the hyper-Laplacian prior to regularize the global spectral structures for multispectral image denoising.

In this paper, we introduce two priors for illumination and reflectance in the Retinex problem which are based on the statistics of corresponding images. For reflectance, we observe from Fig. 1(c) that its gradients fit the hyper-Laplacian distribution well, and use the hyper-Laplacian prior to characterize the gradients of reflectance. For illumination, we observe from Fig. 1(d) that its large gradients fit the hyper-Laplacian distribution well and its small gradients fit the hybrid hyper-Laplacian and Tikhonov distribution well, and use a hybrid regularization combining the hyper-Laplacian and Tikhonov priors to characterize the gradients of illumination.

Based on the priors, we propose a novel variational model for Retinex. Using a logarithmic transformation as in [12] to convert (1) into the logarithmic domain

$$s = l - r, \quad (3)$$

where $s = \log(S)$, $l = \log(L)$, and $r = -\log(R)$. For simplicity, we introduce a point-wise l_2 norm $|\cdot|$. For $x \in \mathbb{R}^{d_1 \times d_2 \times d_3}$, $i = 1, \dots, d_1$, $j = 1, \dots, d_2$, and

$$|x|_{i,j} = \sqrt{\sum_{k=1}^{d_3} x_{i,j,k}^2}.$$

When $d_3 = 1$, $|x| \in \mathbb{R}^{d_1 \times d_2}$ is the same as the point-wise absolute value. The proposed model is then as follows:

$$\begin{aligned} \min_{r,l} \quad & \alpha_1 \| |Dr| \|_{\gamma_1}^{\gamma_1} + \alpha_2 \left\{ \| (1-g) \circ |Dl| \|_{\gamma_2}^{\gamma_2} + \| g \circ |Dl| \|_2^2 \right\} \\ & + \frac{1}{2} \| l - s - r \|_2^2 + \frac{\tau}{2} \| l \|_2^2 + \delta_{\Omega_1}(r) + \delta_{\Omega_2}(l), \end{aligned} \quad (4)$$

where \circ denotes the point-wise multiplication, γ_1 and γ_2 are hyper-Laplacian parameters ($0 < \gamma_1, \gamma_2 < 1$), α_1 and α_2 are two positive regularization parameters, τ is a tiny number that can be set to zero in practice [12], $Dr = (D_1 r, D_2 r) \in \mathbb{R}^{d_1 \times d_2 \times 2}$, and D_1 and D_2 are the discrete difference operators with forward finite-difference scheme along x -direction and y -direction, respectively [31,32]. The first term is the hyper-Laplacian prior for reflectance to describe the sparsity on gradients of reflectance; see details in Section 2.1. The second term is the hybrid regularization term for illumination to describe lightness; see details in Section 2.2. The third term is the data fidelity term. The fourth term is only for the theoretical setting [12] that does not affect the results. The last two terms impose constraints on r and l , respectively, where $\Omega_1 := \{x | x \in \mathbb{R}^{m \times n}, x_{i,j} \geq 0, \forall i, j\}$, $\Omega_2 := \{x | x \in \mathbb{R}^{m \times n}, x_{i,j} \geq s_{i,j}, \forall i, j\}$, m and n are the size of s , $\delta_{\Omega}(X)$ is the indicator function on a nonempty matrix set Ω defined as

$$\delta_{\Omega}(X) = \begin{cases} 0, & \text{if } X \in \Omega, \\ \infty, & \text{otherwise.} \end{cases}$$

Numerically, we solve the proposed model efficiently by the alternating direction method of multipliers (ADMM) [33,34]. Experimental results validate that our method is comparable to state-of-the-art methods both visually and quantitatively.

In summary, the main contributions of this paper are as follows:

- We propose a novel Retinex model by introducing the hyper-Laplacian regularization term for reflectance and the hybrid hyper-Laplacian and Tikhonov term for illumination.
- Experimental results show that the proposed model is comparable to state-of-the-art models in terms of restoring textual details while preventing overexposure.

The rest of this paper is organized as follows. The proposed priors for reflectance and illumination are introduced in Section 2. In Section 3, we present the numerical scheme for solving our model. In Section 4, experiments results are discussed in terms of both performance and quantity. Finally, conclusions are given in Section 5.

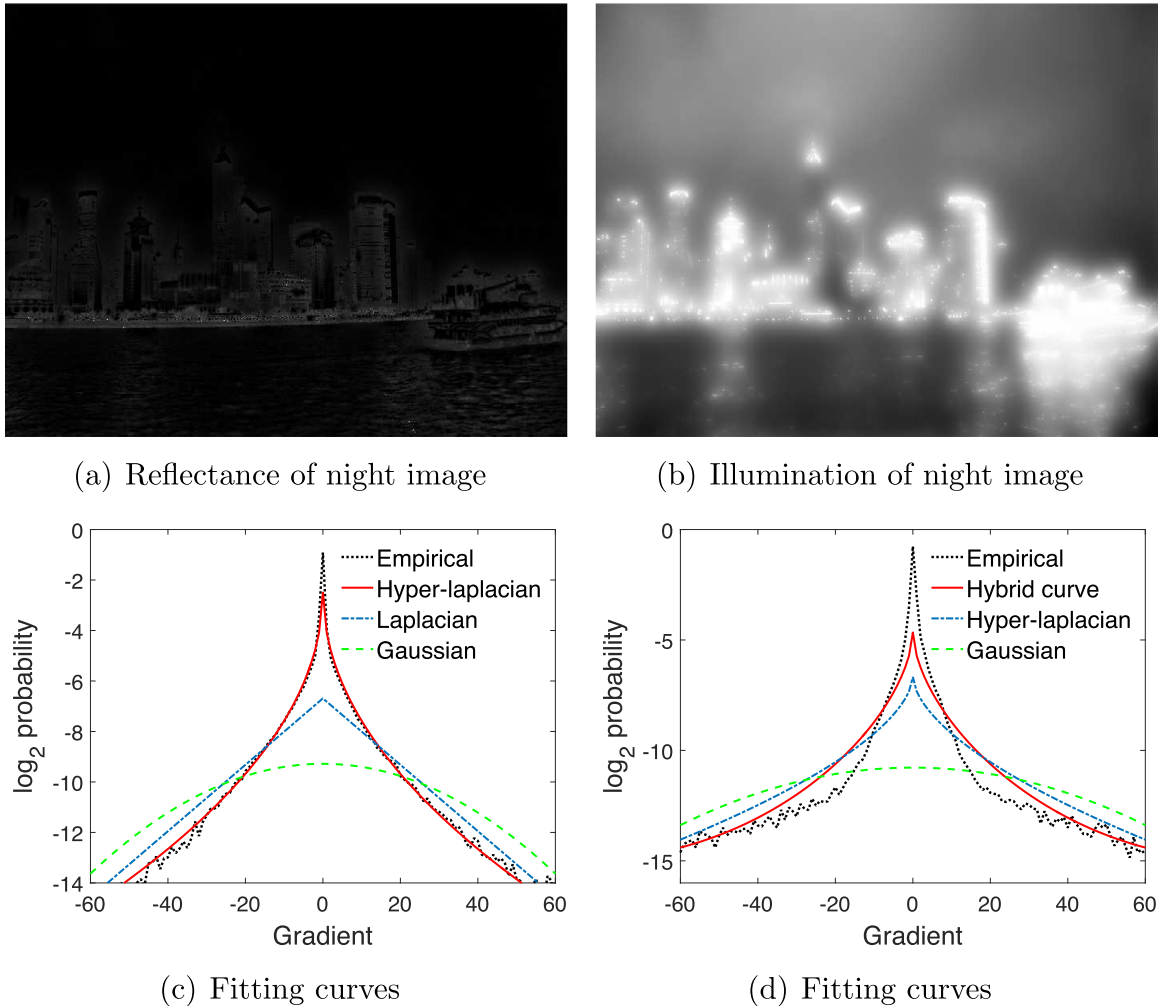


Fig. 1. Decomposition results of night image and the corresponding fitting curves in the gradient domain. (a) Reflectance image. (b) Illumination image. (c) Comparisons among hyper-Laplacian, Gaussian, and Laplacian in fitting the empirical distribution of gradients of reflectance. (d) The empirical distribution of gradients of illumination along with hybrid hyper-Laplacian and Tikhonov, Gaussian, and hyper-Laplacian.

2. Novel reflectance and illumination priors

We illustrate the motivations for the priors of reflectance and illumination in the Retinex problem.

2.1. The reflectance prior

By regularizing the sparsity of the gradient of reflectance, the hyper-Laplacian prior can distinguish different substances in an image to keep details. In gradient field, it is proved that the hyper-Laplacian prior can better model the real-world marginal distribution than the Gaussian and Laplacian [28]. To better understand the superiority of the hyper-Laplacian prior, we present experiments on sets of images under different scenarios to get marginal distributions of their reflectance. Since our Retinex model uses the logarithmic transformation for pre-processing, we put the decomposed results into the logarithmic domain and then analyze their marginal distributions. We utilize three distributions including hyper-Laplacian, Gaussian, and Laplacian to fit the empirical distributions. As we can see in Fig. 2 and 1(c), it is obvious that the hyper-Laplacian prior fits the marginal distribution better than the other two distributions.

2.2. The illumination prior

For illumination, our hybrid regularization term combines the advantages of the hyper-Laplacian and Tikhonov. The hyper-Laplacian prior is superior to describe the edges of different lightness regions. While the Tikhonov prior is effective in simulating the light intensity and removing details. Therefore, we combine the two priors together to describe different

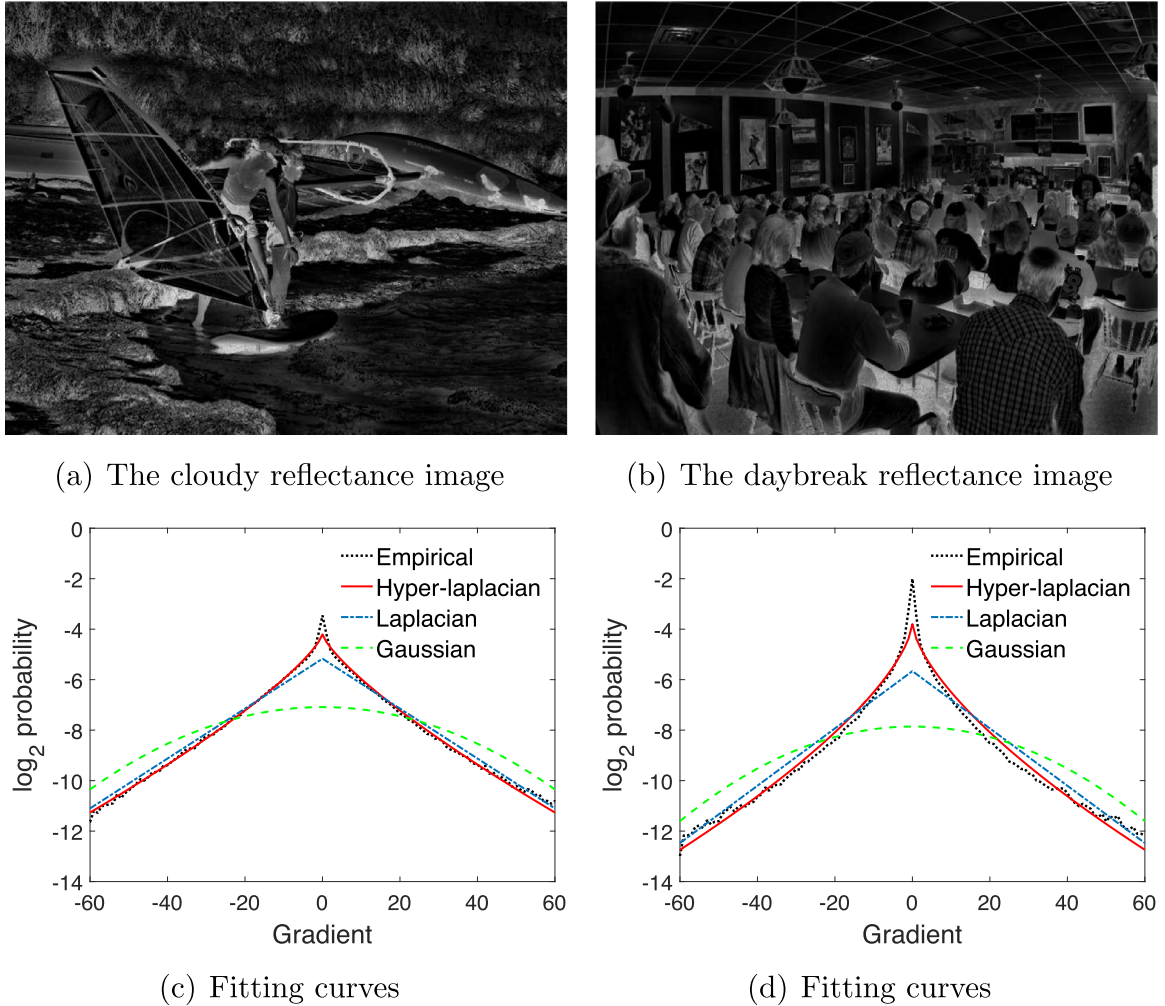


Fig. 2. The comparisons among hyper-Laplacian (red), Laplacian (green), and Gaussian (blue) in fitting the empirical distribution (black) of reflectance in different scenarios including cloudy and daybreak. (For interpretation of the references to color in this figure legend, the reader is referred to the web version of this article.)

lightness regions and eliminate details. Like the reflectance case, we analyze the marginal distributions of illumination in Figs. 3 and 1(d). We compare our hybrid regularization term with the hyper-Laplacian and Gaussian. The results suggest that the hybrid hyper-Laplacian and Tikhonov describes the large gradients as effectively as the hyper-Laplacian, but fits the small gradients better than the hyper-Laplacian and Gaussian. Therefore, it is reasonable to combine the two priors together to regularize the illumination.

We make some comments on the hybrid regularization term

$$\alpha_2 \{ \| (1-g) \circ |Dl| \|_{\gamma_2}^{\gamma_2} + \| g \circ |Dl| \|_2^2 \}, \quad (5)$$

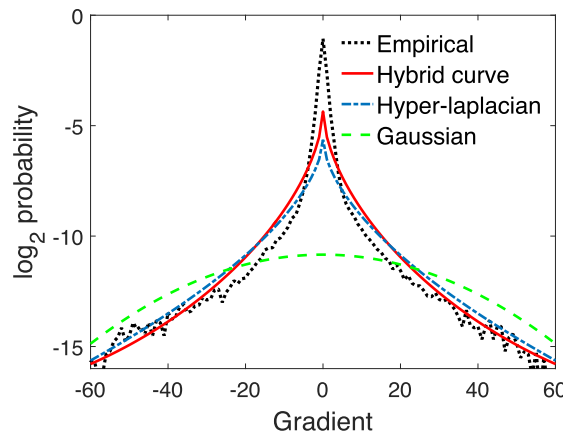
where \circ denotes the point-wise multiplication, α_2 is the regularization parameter; $\| \cdot \|_{\gamma_2}^{\gamma_2}$ is the hyper-Laplacian prior; γ_2 is the parameter with $0 < \gamma_2 < 1$; g is the adaptive point-wise coefficient $g = \frac{1}{1+\mu+\eta|\nabla s|^2}$; μ is the parameter to ensure $g < 1$ and we set to 10^{-6} as default; η is a positive parameter controlling the proportion of ∇s ; ∇s is the gradient of initial image s . The coefficient g balances the two terms. On one hand, when ∇s is large, g is small. The hyper-Laplacian prior plays an important role to describe edges well. On the other hand, the Tikhonov regularization term keeps the smoothness of objects when ∇s is small (g is large). Therefore, we not only distinguish the different light intensity regions well, but also reserve the smoothness to get rid of details and keep the regions smooth.



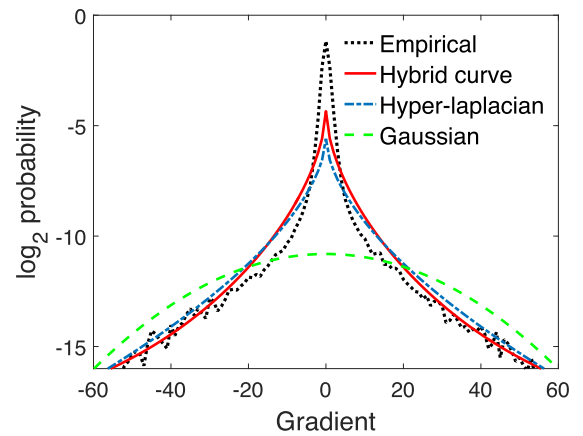
(a) The cloudy illumination image



(b) The daybreak illumination image



(c) Fitting curves



(d) Fitting curves

Fig. 3. The comparisons among hybrid hyper-Laplacian and Tikhonov (red), hyper-Laplacian (blue), and Gaussian (green) in fitting the empirical distribution (black) of illumination in different scenarios including cloudy and daybreak. (For interpretation of the references to color in this figure legend, the reader is referred to the web version of this article.)

3. The numerical algorithm

This section presents the existence of a minimizer of energy (4) and the details of using the alternating direction method of multipliers (ADMM) to solve the proposed model.

3.1. The ADMM framework

First, we give a theorem to show that the energy of (4) has at least one solution.

Theorem 1. *The model (4) has at least one minimizer.*

Proof. We use $E(r, l)$ to denote the objective function (4). It is clear that $E(r, l)$ is proper and continuous. According to the Weierstrass' theorem [35], it remains only to show the coercivity of $E(r, l)$, i.e., for every sequence $\{(r^i, l^i)\}$ such that

$$\|r^i\|_2 + \|l^i\|_2 \rightarrow \infty,$$

we have

$$\lim_{i \rightarrow \infty} E(r^i, l^i) = \infty.$$

Algorithm 1 ADMM algorithm for solving (6).

Require: ϵ_l , α_1 , α_2 , γ_1 , γ_2 , μ , η , and s .

Ensure: l and r .

while stopping criterion $\frac{\|l^{k+1} - l^k\|}{\|l^{k+1}\|} \leq \epsilon_l$ is not satisfied **do**

Step 1. Computing u^{k+1} , v^{k+1} , w^{k+1} , h^{k+1} , and q^{k+1} by solving

$$\arg \min_{u,v,w,h,q} \mathcal{L}(u, v, w, h, q, l^k, r^k, \lambda^k). \quad (5)$$

Step 2. Computing l^{k+1} and r^{k+1} by solving

$$\arg \min_{l,r} \mathcal{L}(u^{k+1}, v^{k+1}, w^{k+1}, h^{k+1}, q^{k+1}, l, r, \lambda^k). \quad (5)$$

Step 3. Update λ_1^{k+1} , λ_2^{k+1} , λ_3^{k+1} , λ_4^{k+1} and λ_5^{k+1} by

$$\begin{aligned} \lambda_1^{k+1} &\leftarrow \lambda_1^k + \beta(u^{k+1} - Dl^{k+1}), \\ \lambda_2^{k+1} &\leftarrow \lambda_2^k + \beta(v^{k+1} - Dr^{k+1}), \\ \lambda_3^{k+1} &\leftarrow \lambda_3^k + \beta(w^{k+1} - Dr^{k+1}), \\ \lambda_4^{k+1} &\leftarrow \lambda_4^k + \beta(h^{k+1} - r^{k+1}), \\ \lambda_5^{k+1} &\leftarrow \lambda_5^k + \beta(q^{k+1} - l^{k+1}). \end{aligned} \quad (5)$$

end while

We prove it by contradiction. Suppose that there exists a subsequence of $\{(r^i, l^i)\}$ (also denoted as $\{(r^i, l^i)\}$) that $\{E(r^i, l^i)\}$ is bounded. Denote

$$E_1(r, l) = \frac{1}{2}(l^i - r^i - s)^2.$$

Since $\{E(r^i, l^i)\}$ is bounded, it is clear that the sequences $\{\|l^i\|_2^2\}$, and $\{E_1(r^i, l^i)\}$ are bounded, and we have $\{|l^i|\}$ is bounded. Note that

$$(r^i)^2 = (r^i - (l^i - s) + (l^i - s))^2 \leq 2(r^i - (l^i - s))^2 + 2(l^i - s)^2$$

Since $\{E_1(r^i, l^i)\}$ and $\{|l^i|\}$ are bounded, $\{|r^i|\}$ is bounded. Then we have $\{\|r^i\|_2\}$ and $\{\|l^i\|_2\}$ are bounded, which is a contradiction. \square

We now use ADMM to solve the optimization problems because of its convergence and speed [36–38]. To utilize the ADMM framework, we first introduce auxiliary variables u , v , w , h , and q to rewrite the proposed model as follows:

$$\begin{aligned} \min_{u,v,w,h,q,r,l} & \alpha_1 \|w\|_{\gamma_1}^{\gamma_1} + \alpha_2 \left\{ \|(1-g) \circ |u|\|_{\gamma_2}^{\gamma_2} + \|g \circ |v|\|_2^2 \right\} \\ & + \frac{1}{2} \|l - s - r\|_2^2 + \frac{\tau}{2} \|l\|_2^2 + \delta_{\Omega_1}(h) + \delta_{\Omega_2}(q), \\ & \text{s.t. } w = Dr, \quad u = Dl, \quad v = Dr, \quad h = r, \quad q = l. \end{aligned} \quad (9)$$

In order to handle the linear constraints, we consider the following augmented Lagrangian function of (6):

$$\begin{aligned} \mathcal{L}(u, v, w, h, q, l, r, \lambda_1, \lambda_2, \lambda_3, \lambda_4, \lambda_5) &= \alpha_1 \|w\|_{\gamma_1}^{\gamma_1} + \alpha_2 \left\{ \|(1-g) \circ |u|\|_{\gamma_2}^{\gamma_2} + \|g \circ |v|\|_2^2 \right\} \\ & + \frac{1}{2} \|l - r - s\|_2^2 + \frac{\tau}{2} \|l\|_2^2 + \delta_{\Omega_1}(h) + \delta_{\Omega_2}(q) + \langle \lambda_1, u - Dl \rangle + \langle \lambda_2, v - Dr \rangle \\ & + \langle \lambda_3, w - Dr \rangle + \langle \lambda_4, h - r \rangle + \langle \lambda_5, q - l \rangle + \frac{\beta}{2} \|u - Dl\|_2^2 \\ & + \frac{\beta}{2} \|v - Dr\|_2^2 + \frac{\beta}{2} \|w - Dr\|_2^2 + \frac{\beta}{2} \|h - r\|_2^2 + \frac{\beta}{2} \|q - l\|_2^2, \end{aligned} \quad (10)$$

where $\lambda_1, \lambda_2, \lambda_3, \lambda_4$ and λ_5 are Lagrangian multipliers, and $\beta > 0$ is a penalty parameter for the linear constraints [39]. The variables in (7) are separated into two groups (u, v, w, h, q) and (l, r) decoupled in the objective and the linear constraints.

The iterative process of ADMM is shown in Algorithm 1. In each iteration, we minimize the objective function with respect to the two groups alternatively followed by updates of the Lagrangian multipliers.

3.2. The subproblems

We present the details for solving each subproblem in Algorithm 1.

Step 1. In this step we solve the (u, v, w, h, q) subproblems. The minimizations with respect to u, v, w, h , and q can be solved separately since the variables are decoupled from each other.

The u -subproblem is given by

$$\arg \min_u \alpha_2 \| (1-g) \circ |u| \|_{\gamma_2}^{\gamma_2} + \frac{\beta}{2} \left\| u - Dl + \frac{\lambda_1}{\beta} \right\|_2^2. \quad (11)$$

The u -subproblem can be efficiently solved by the generalization of soft-thresholding (GST) [40] operator using one iteration as follows:

$$[u_t]_{i,j}^{k+1} = \begin{cases} 0, & \text{if } \xi_{i,j,t}^k \leq \psi_{i,j}, \\ \operatorname{sgn}(\xi_{i,j,t}^k) \left[|\xi_{i,j,t}^k| - \frac{\gamma_2 \alpha_2 (1-g)_{i,j}}{\beta} (|\xi_{i,j,t}^k|)^{\gamma_2-1} \right], & \text{otherwise,} \end{cases} \quad (12)$$

where k denotes the k th iteration, $t = 1, 2$ and we set $\xi_{i,j,t}^k = (Dl^k - \frac{\lambda_1^k}{\beta})_{i,j,t}$ for convenience, $\operatorname{sgn}(\xi_{i,j,t}^k)$ denotes the sign of $\xi_{i,j,t}^k$, and the threshold $\psi_{i,j}$ is determined by

$$\psi_{i,j} = \left[\frac{2\alpha_2(1-g)_{i,j}}{\beta} (1-\gamma_2) \right]^{\frac{1}{2-\gamma_2}} + \frac{\alpha_2(1-g)_{i,j}}{\beta} \gamma_2 \left[\frac{2\alpha_2(1-g)_{i,j}}{\beta} (1-\gamma_2) \right]^{\frac{\gamma_2-1}{2-\gamma_2}}. \quad (13)$$

In this work, the convergence of GST can be guaranteed [40], and the solution is more stationary and accurate than other methods.

The v -subproblem is given by

$$\arg \min_v \alpha_2 \| g \circ |v| \|_2^2 + \frac{\beta}{2} \left\| v - Dl + \frac{\lambda_2}{\beta} \right\|_2^2, \quad (14)$$

whose solution is given by

$$[v_t]_{i,j}^{k+1} = \frac{(\beta Dl^k - \lambda_2^k)_{i,j,t}}{\beta + 2\alpha_2(g)_{i,j}}, \quad \text{for } t = 1, 2. \quad (15)$$

The w -subproblem is given by

$$\arg \min_w \alpha_1 \| |w| \|_{\gamma_1}^{\gamma_1} + \frac{\beta}{2} \left\| w - Dr + \frac{\lambda_3}{\beta} \right\|_2^2. \quad (16)$$

The w subproblem can be also solved by the GST [40] operator using one iteration as follows:

$$[w_t]_{i,j}^{k+1} = \begin{cases} 0, & \text{if } \rho_{i,j,t}^k \leq \varphi, \\ \operatorname{sgn}(\rho_{i,j,t}^k) \left[|\rho_{i,j,t}^k| - \frac{\gamma_1 \alpha_1}{\beta} (|\rho_{i,j,t}^k|)^{\gamma_1-1} \right], & \text{otherwise,} \end{cases} \quad (17)$$

where $t = 1, 2$ and $\rho_{i,j,t}^k = (Dr^k - \frac{\lambda_3^k}{\beta})_{i,j,t}$ and the threshold φ is determined by

$$\varphi = \left[\frac{2\alpha_1}{\beta} (1-\gamma_1) \right]^{\frac{1}{2-\gamma_1}} + \frac{\gamma_1 \alpha_1}{\beta} \left[\frac{2\alpha_1}{\beta} (1-\gamma_1) \right]^{\frac{\gamma_1-1}{2-\gamma_1}}. \quad (18)$$

The h -subproblem is given by

$$\arg \min_h \frac{\beta}{2} \left\| h - r + \frac{\lambda_4}{\beta} \right\|_2^2 + \delta_{\Omega_1}(h). \quad (19)$$

The solution is as follows:

$$[h]_{i,j}^{k+1} = \max \left\{ r_{i,j}^k - \frac{\lambda_4^k}{\beta}, 0 \right\}. \quad (20)$$

The q -subproblem is given by

$$\arg \min_q \frac{\beta}{2} \left\| q - l + \frac{\lambda_5}{\beta} \right\|_2^2 + \delta_{\Omega_2}(q). \quad (21)$$

The solution is as follows:

$$[q]_{i,j}^{k+1} = \max \left\{ l_{i,j}^k - \frac{\lambda_5^k}{\beta}, s_{i,j} \right\}. \quad (22)$$

Step 2. In this step we solve the (l, r) subproblem. The (l, r) subproblem is given by

$$\begin{aligned} \arg \min_{l,r} \frac{1}{2} \|l - r - s\|_2^2 + \frac{\tau}{2} \|l\|_2^2 + \frac{\beta}{2} \left\| u - Dl + \frac{\lambda_1}{\beta} \right\|_2^2 + \frac{\beta}{2} \left\| v - Dl + \frac{\lambda_2}{\beta} \right\|_2^2 \\ + \frac{\beta}{2} \left\| w - Dr + \frac{\lambda_3}{\beta} \right\|_2^2 + \frac{\beta}{2} \left\| h - r + \frac{\lambda_4}{\beta} \right\|_2^2 + \frac{\beta}{2} \left\| q - l + \frac{\lambda_5}{\beta} \right\|_2^2. \end{aligned} \quad (23)$$

We solve l and r jointly. The optimality condition gives the following linear system

$$\begin{bmatrix} M_1 & M_3^T \\ M_3 & M_2 \end{bmatrix} \begin{bmatrix} l \\ r \end{bmatrix} = \begin{bmatrix} B_1 \\ B_2 \end{bmatrix}, \quad (24)$$

where the block matrices are defined as

$$\begin{cases} M_1 = I + 2\beta \sum_{t=1}^2 D_t^T D_t + \beta + \tau, \\ M_2 = I + \beta \sum_{t=1}^2 D_t^T D_t + \beta, \\ M_3 = -I, \end{cases} \quad (25)$$

and

$$B_1 = s + \beta \left[\sum_{t=1}^2 D_t^T \left(u^k + \frac{\lambda_1^k}{\beta} \right) + \sum_{t=1}^2 D_t^T \left(v^k + \frac{\lambda_2^k}{\beta} \right) + q^k + \frac{\lambda_5^k}{\beta} \right], \quad (26)$$

and

$$B_2 = -s + \beta \left[\sum_{t=1}^2 D_t^T \left(w^k + \frac{\lambda_3^k}{\beta} \right) + h^k + \frac{\lambda_4^k}{\beta} \right]. \quad (27)$$

We solve (21) in the Fourier domain. F and F^* are the matrix forms representing the discrete Fourier transform and the corresponding inverse transform, respectively. By denoting $\tilde{M}_j = \text{diag}(FM_jF^*)$ and $\tilde{M}_j^T = \text{diag}(FM_j^TF^*)$, we obtain

$$\begin{cases} \tilde{M}_1 \circ (Fl) + \tilde{M}_3^T \circ (Fr) = FB_1, \\ \tilde{M}_3 \circ (Fl) + \tilde{M}_2 \circ (Fr) = FB_2, \end{cases} \quad (28)$$

where \circ is componentwise multiplication. Similarly to the scalar case, Fl and Fr can be obtained by Cramer's rule. The solutions are as follows:

$$l = F^* \left(\left| \begin{array}{cc} FB_1 & \tilde{M}_3^T \\ FB_2 & \tilde{M}_2 \end{array} \right|_* \middle/ \left| \begin{array}{cc} \tilde{M}_1 & \tilde{M}_3^T \\ \tilde{M}_3 & \tilde{M}_2 \end{array} \right|_* \right), \quad (29)$$

and

$$r = F^* \left(\left| \begin{array}{cc} \tilde{M}_1 & FB_1 \\ \tilde{M}_3 & FB_2 \end{array} \right|_* \middle/ \left| \begin{array}{cc} \tilde{M}_1 & \tilde{M}_3^T \\ \tilde{M}_3 & \tilde{M}_2 \end{array} \right|_* \right), \quad (30)$$

where the division is componentwise. $|\cdot|_*$ is defined as

$$\left| \begin{array}{cc} a_{11} & a_{12} \\ a_{21} & a_{22} \end{array} \right|_* = a_{11} \circ a_{22} - a_{12} \circ a_{21}, \quad (31)$$

where $a_{ij} \in \mathbb{R}^{m \times n}$.

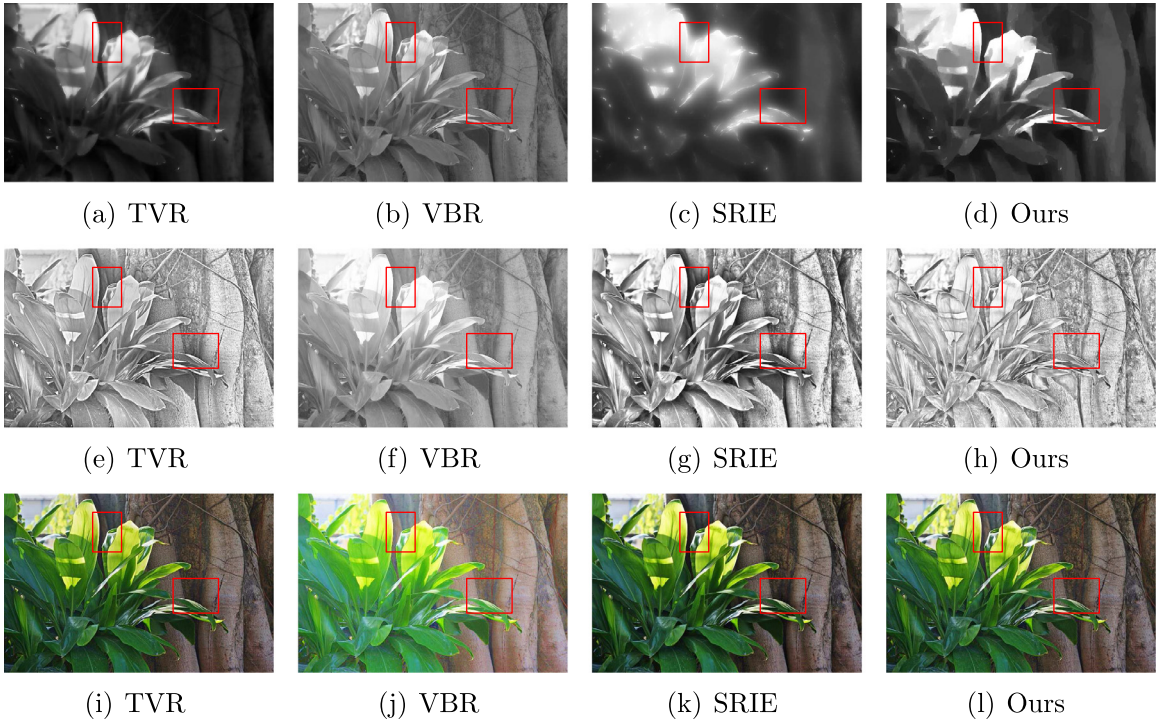


Fig. 4. The illumination (top row), reflectance (middle row), and enhanced results (bottom row) by different methods. First column: TVR. Second column: VBR. Third column: SRIE. Fourth column: the proposed method.

4. Numerical experiments

We compare the proposed model with the state-of-the-art methods, including [12–14,41]. Section 4.1 analyzes the reflectance and illumination decomposed by our method and the competing methods. Section 4.2 compares our final enhanced results with the competing methods in qualitative and quantitative ways. In our experiments, we apply the proposed method in the HSV domain, which contains three layers: Hue (H), Saturation (S), and Value (V). The H channel and the S channel convey most color information, and the V channel stands for the brightness of objects. Therefore, we perform our method only on the V channel and then transform the enhanced result back to the RGB color space to get the final result. All experiments are conducted under Windows 7 and Matlab R2013b running on a desktop with an Intel(R) Core (TM) i3-2130 CPU at 3.40GHz and 4GB memory.

Parameter setting. Our method involves the following parameters: α_1 , α_2 , μ , η , γ_1 , γ_2 , τ , and β in model (4). α_1 controls the reflectance and we set it to 0.01. α_2 controls the illumination and we set it to 0.7. μ and η control the adaptive coefficient g in (5), and we set $\mu = 10^{-6}$, $\eta = 80$. τ is only for the theoretical setting. The results are not affected significantly by τ [12] and we set $\tau = 10^{-6}$. We will discuss α_1 , α_2 , and η in Section 4.3 in details. γ_1 and γ_2 are the parameters to control the sparsity of hyper-Laplacian and we set as 0.6 and 0.75, respectively. And the penalty parameter β chosen as 10 controls the speed of convergence.

Competing methods. We choose four state-of-the-art competing methods including the Total Variation model for Retinex (TVR) [12], the Variational model with Barrier functionals for Retinex (VBR) [13], the Simultaneous Reflection and Illumination Estimation (SRIE) [14], and the Naturalness Preserved Enhancement algorithm (NPE) [41]. TVR uses the Tikhonov regularization for illumination and TV regularization for reflectance. VBR is based on TVR and adds some constraints on variables. The above two methods are based on the log transformation and SRIE proposes a weighted variational model to overcome the limit of the log transformation. And NPE gets the details in reflectance by a bright-pass filter. All the parameters in the competing methods are chosen according to their original essays.

Evaluation indices. We quantitatively evaluate the enhanced results by two indices: the natural image quality evaluator (NIQE) [42] and the lightness order error (LOE) [41]. NIQE represents the quality of an image without extra images by using the natural scene statistic (NSS) feathers from a corpus of natural images and fitting them with a multivariate Gaussian (MVG) model. NIQE is defined as

$$D(\nu_1, \nu_2, \Sigma_1, \Sigma_2) = \sqrt{\left((\nu_1 - \nu_2)^T \left(\frac{\Sigma_1 + \Sigma_2}{2} \right)^{-1} (\nu_1 - \nu_2) \right)}, \quad (32)$$

where v_1, v_2 are the mean vectors of the natural MVG model and the distorted MVG model, respectively, while Σ_1, Σ_2 are the covariance matrices of the two models. A high quality image usually has a low value of NIQE. LOE is used to assess the naturalness preservation, especially the lightness varieties and light source directions. LOE contrasts the original image I and the enhanced image I_e , and it defines as follows:

$$\text{LOE} = \frac{1}{mn} \sum_{i=1}^m \sum_{j=1}^n \text{RD}(i, j), \quad (33)$$

where m, n are the size of the image. $\text{RD}(i, j)$ is the relative order at the pixel (i, j) and is defined by

$$\text{RD}(x, y) = \sum_{i=1}^m \sum_{j=1}^n \left(U(L(x, y), L(i, j)) \oplus U(L_e(x, y), L_e(i, j)) \right), \quad (34)$$

and

$$U(x, y) = \begin{cases} 1, & \text{if } x \geq y, \\ 0, & \text{otherwise,} \end{cases}$$

where $U(x, y)$ is the unit step function and \oplus is the exclusive-or operator. The lower LOE is, the more naturalness an image preserves. As the important criteria, naturalness is defined in [43] as follows: the ambience of image should not be changed greatly after enhancement, and no additional light source should be introduced to the scene, and no halo effect should be added and no blocking effect should be amplified due to over-enhancement. It suggests that we should not over-enhance an image by simply increasing the intensity of lightness, and it is unnatural to explore more detail information by introducing artifacts.

4.1. Comparisons in illumination and reflectance

We compare our decomposed results illumination and reflectance with other methods, and elucidate how they affect the final enhanced results. Fig. 4 shows the reflectance images, illumination images, and enhanced results by different methods.

Illumination. The illumination reveals the varieties of lightness while distinguishing the main edges of lightness. In Fig. 4(a)–(d), we observe that the illumination images by TVR and VBR have too many details which destroy the essence of illumination. As for SRIE, it faithfully obeys the smoothness prior of illumination, but ignores the edge regions of two different lightness parts. As indicated by the red rectangular mark in Fig. 4(c), there are two distinct lightness areas but SRIE does not differentiate them clearly. In Fig. 4(d), the illumination result by the proposed model nearly has no details such as the trunk and can distinguish different lightness regions clearly.

Reflectance. The reflectance should contain only detail information without lightness changing. In Fig. 4(e) and (f), the reflectance results by TVR and VBR contain few details because they are taken away by the illumination. In the marked rectangular areas in Fig. 4(g), the reflectance image by SRIE has conspicuous dark regions which are caused by the smoothness prior in illumination. Our results shown in Fig. 4(h) is clear and get more useful information in the marked rectangular areas compared with Fig. 4(g). Furthermore, the texture on the leaves and spots on the trunk are reflected better by the proposed method than others.

In summary, our reflectance image has more details than the other methods; our illumination image is smooth in the inner part, while the edges can be distinguished well. The final results shown in the third row of Fig. 4 further indicate the impact of illumination. Fig. 4(j) looks over-exposed because the illumination is too clear, which makes the reflectance lose many fine details. Compared with Fig. 4(i) and (k), our result shown in Fig. 4(l) is more obvious in edge areas and gets more information that is covered by shadow regions in the marked red rectangular.

4.2. Comparisons in enhanced results

We compare different methods on the cloudy sky, daybreak, and night, which are shown in Figs. 5–7, respectively.

Fig. 5 shows the experiments under a cloudy sky. TVR and SRIE can not restore the colors of the trees and the white building. VBR is over-exposed on the whole lightness shown in Fig. 5(c). NPE and the proposed method conform to the naturalness. However, NPE over-enhances some areas such as trees in front of the white building.

Fig. 6 displays the experiments at daybreak. As we can see, NPE shown in Fig. 6(d) over-enhances on the blue coat and jeans, making the color become white like VBR in Fig. 6(c). TVR and SRIE shown in Fig. 6(b) and (e), respectively, have unexpected dark regions on the sea since the contrast between the sunshine and sea is high. Our method handles this high contrast well to remove the shadows in Fig. 6(f) and does not make excessive enhancement.

Fig. 7 presents the situation at night and we still achieve the best performance. The proposed method gets more information on the books covered by shadows shown in Fig. 7(f) compared with TVR in Fig. 7(b) and SRIE in Fig. 7(e). Fig. 7(c) shows that VBR is overexposed on the left rectangular area. Although NPE presented in Fig. 7(d) is more clear in the letters on the book, the left grass in the background becomes white and loses its original color. This kind of over enhancement is serious and can be reflected in the indices which we will present later.

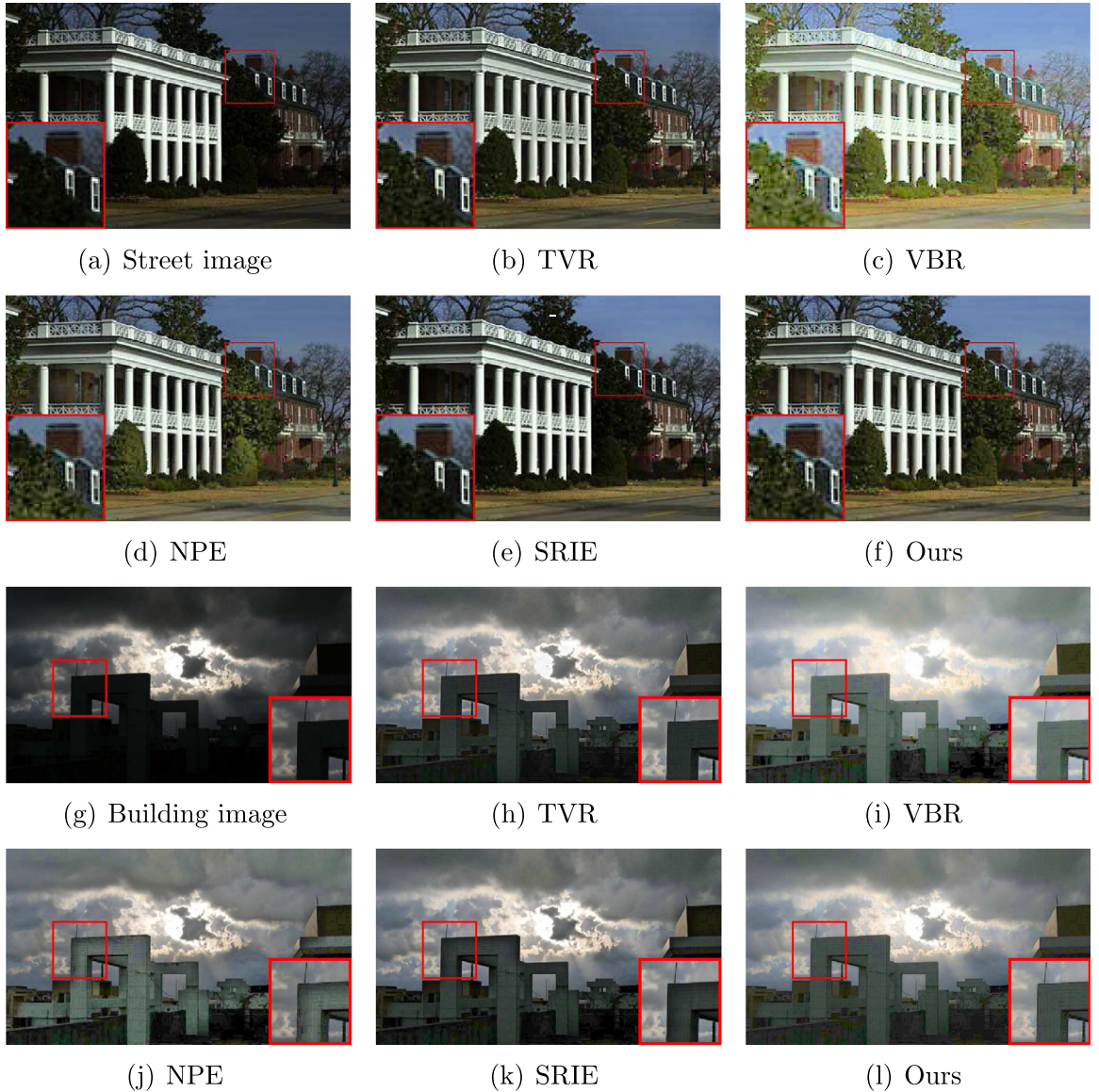


Fig. 5. The input images (street and building) under a cloudy sky and enhanced results by different methods.

In summary, the competing methods are limited in preserving details and prevent the overexposure simultaneously, whereas the proposed method is able to balance the details and overexposure well. We can see that VBR often causes overexposed problems. TVR can handle the lightness order well, but it loses some details in the edge of high contrast regions. NPE has high contrast and preserves naturalness. However, the results will be over enhanced in some regions because of the high contrast. SRIE has better visual effect than TVR and performs well in above situations. Therefore, we further test some experiments to compare our method and SRIE. In Fig. 8, we show some under-exposed images. It is obvious that SRIE does not improve much and looks fuzzy in Fig. 8(b) and (e). Nevertheless, the proposed method can keep texture and naturalness while increasing lightness.

Table 1 presents the NIQE [42] and LOE [41] values of different methods in the experiments. The proposed method has the lowest NIQE and LOE values in average, which means that our results have the highest quality and looks natural. It is worth noticing that our LOE value is one fifth of SRIE which is the second lowest.

The convergence results of many algorithms have been established in the field of nonconvex optimization [44,45]. We have carefully studied those works and found that most convergence results rely on some assumptions on the problem, which are, however, not available for our model. Unfortunately, we have not succeeded in giving a rigorous proof of the convergence, and that will be considered as future work.

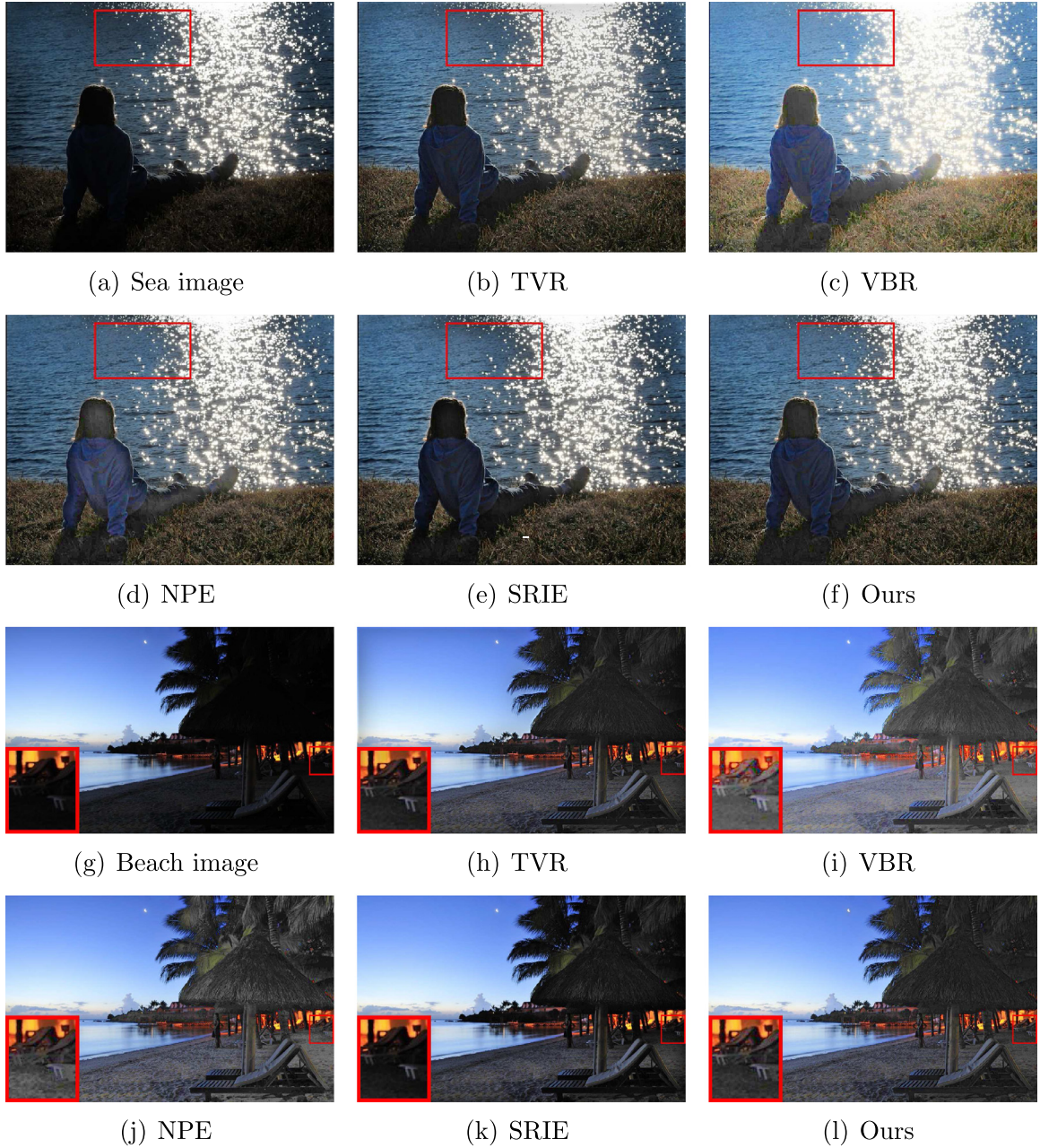


Fig. 6. The input images (sea and beach) at daybreak and enhanced results by different methods.

4.3. The parameter discussion

There are three main parameters in our model (4): α_1 controls the reflectance, α_2 controls the illumination, and η controls the adaptive weighted coefficient g which detects the edge of an image. In Figs. 9–11, we investigate the effects of α_1 , α_2 , and η , respectively.

Fig. 9 suggests that with the increasing of α_1 , the reflectance becomes smooth and loses details while the illumination is clear. Fig. 10 presents the results of illumination with α_2 changing from 0.1 to 1.5. The illumination map is getting fuzzy, and regions with different lightness are well distinguished as α_2 increases. Nonetheless, the illumination becomes so smooth that it can not recognize the edges when α_2 is 1.5, particularly in eyes and walls. In Fig. 11, the varieties of images are

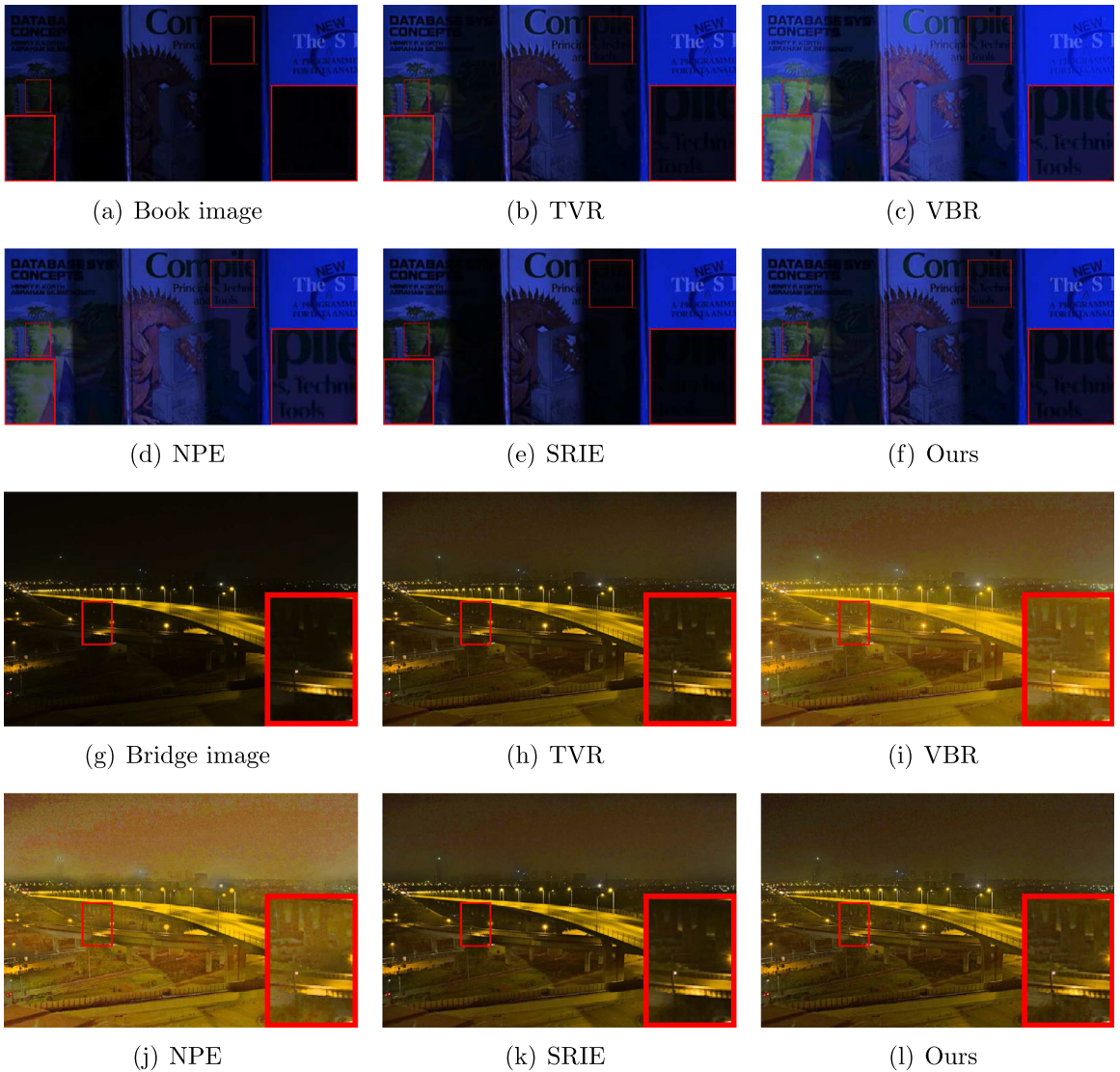


Fig. 7. The input images (book and bridge) at night and enhanced results by different methods.

Table 1
Quantitative comparisons of different methods in terms of NIQE and LOE. The best result is highlighted in bold.

Situation	Image	Index	TVR	VBR	NPE	SRIE	Ours
Cloudy	Street	NIQE	4.63	21.33	4.32	4.66	4.50
		LOE	251.41	530.86	224.54	234.39	88.08
	Building	NIQE	3.32	19.88	3.37	3.72	2.87
		LOE	208.81	1684.30	533.81	108.01	33.62
Daybreak	Sea	NIQE	2.27	17.58	2.29	2.34	2.22
		LOE	125.11	208.10	85.46	194.10	48.24
	Beach	NIQE	2.43	18.94	2.32	2.53	2.22
		LOE	224.91	253.05	221.87	215.87	38.25
Night	Book	NIQE	4.79	20.71	4.70	4.58	4.65
		LOE	136.70	1068.70	196.08	156.02	40.79
	Bridge	NIQE	3.31	19.47	3.14	3.36	3.13
		LOE	459.97	1060.01	1118.40	492.33	43.53
Average	NIQE	3.46	19.65	3.36	3.53	3.26	
	LOE	234.49	800.84	396.69	233.45	48.75	

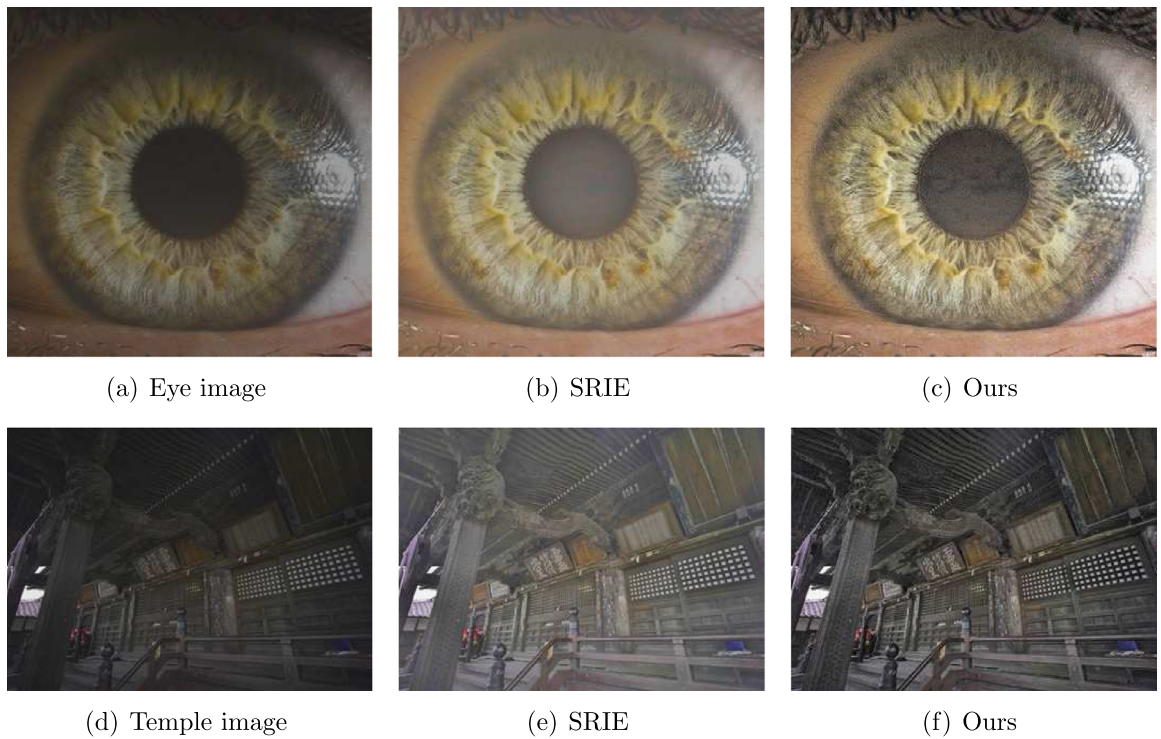


Fig. 8. The input under-exposed images (eye and temple) and enhanced results comparison between SRIE and the proposed method.

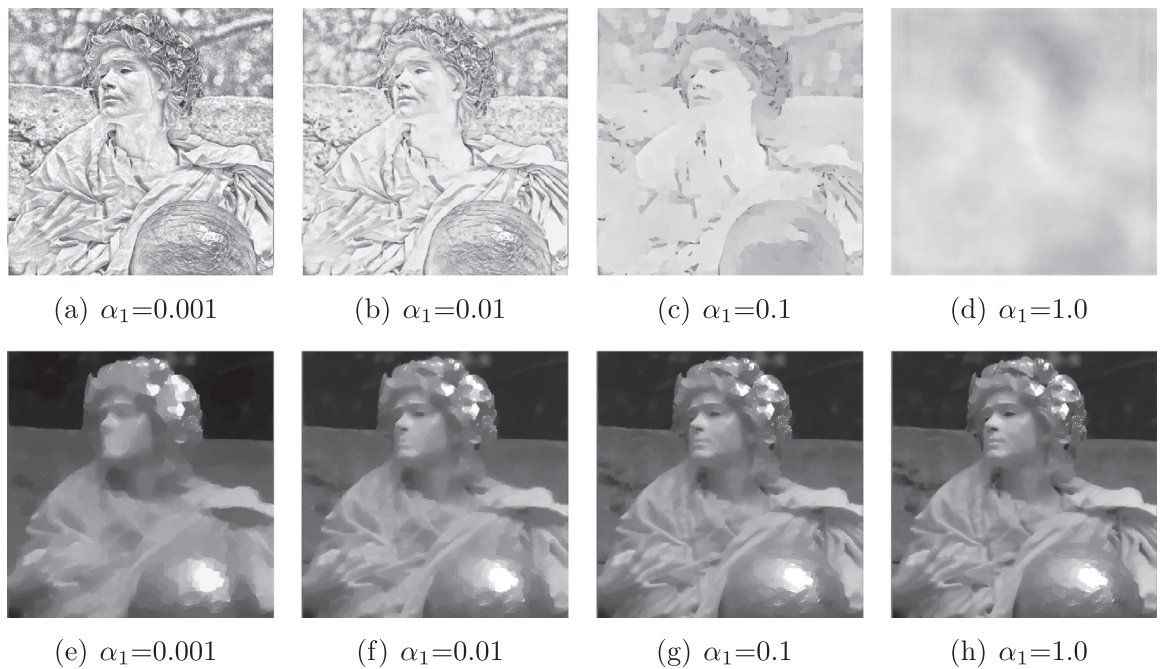


Fig. 9. The reflectance (top row) and illumination (bottom row) results by changing α_1 from 0.001 to 1.0.

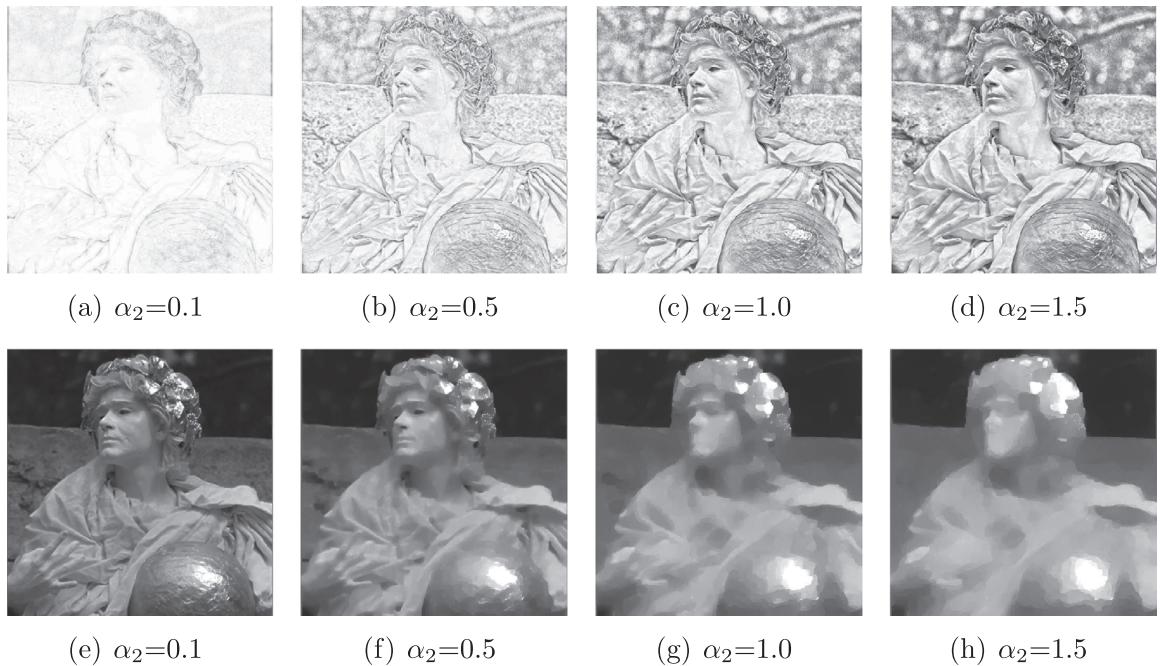


Fig. 10. The reflectance (top row) and illumination (bottom row) results by changing α_2 from 0.1 to 1.5.

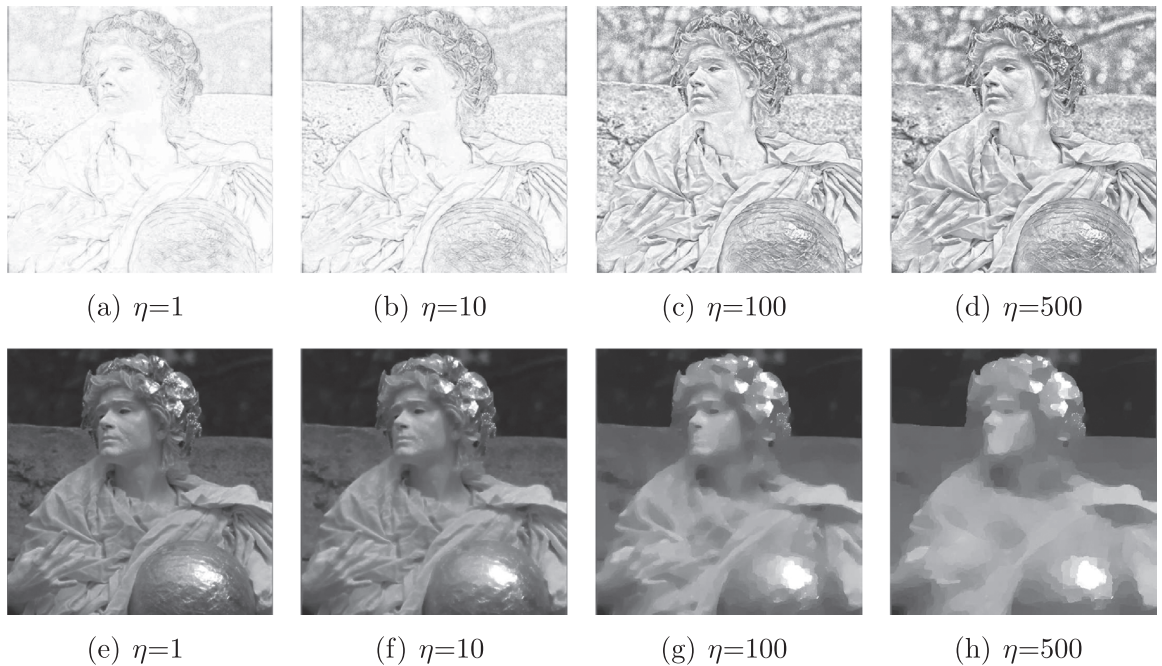


Fig. 11. The reflectance (top row) and illumination (bottom row) results by changing η from 1 to 500.

closely with Fig. 10 since the η controls the illumination as α_2 does. When η is small, the illumination becomes smooth. The different regions are becoming clear, and details are removed well as η increases.

5. Conclusion

We propose a Retinex model by introducing novel reflectance and illumination priors in the Retinex problem. For reflectance, we use the hyper-Laplacian prior to describe the sparsity of the gradient. For illumination, we combine the hyper-Laplacian and Tikhonov regularizations together to distinguish the edges of different lightness regions as well as keeping lightness regions smooth. The ADMM framework is applied to solve the proposed model. In numerical experiments, we use two indices including NIQE and LOE to measure both the quality of images and the naturalness of the enhanced results. Besides, we test our method in different scenarios and get good performance compared with state-of-the-art methods.

Acknowledgments

This research is supported by the National Science Foundation of China (61772003, 61876203), the Fundamental Research Funds for the Central Universities (ZYGX2016J132), Science Strength Promotion Programme of UESTC.

References

- [1] E.H. Land, J.J. McCann, Lightness and Retinex theory, *J. Opt. Soc. Am. A* 61 (1) (1971) 1–11.
- [2] E.H. Land, Color vision and the natural image. Part I, *Proc. Nat. Acad. Sci. USA* 45 (1) (1959) 115.
- [3] E.H. Land, Recent advances in retinex theory and some implications for cortical computations: color vision and the natural image, *Proc. Nat. Acad. Sci.* 80 (16) (1983) 5163–5169.
- [4] E. Provenzi, L.D. Carli, A. Rizzi, D. Marini, Mathematical definition and analysis of the Retinex algorithm, *J. Opt. Soc. America A* 22 (12) (2005) 2613–2621.
- [5] T.J. Cooper, F.A. Baqai, Analysis and extensions of the Frankle-McCann Retinex algorithm, *J. Electr. Imaging* 13 (1) (2004) 85–92.
- [6] E.H. Land, An alternative technique for the computation of the designator in the retinex theory of color vision, *Proc. Nat. Acad. Sci.* 83 (10) (1986) 3078–3080.
- [7] B.K.P. Horn, Determining lightness from an image, *Comput. Graph. Image Process.* 3 (4) (1974) 277–299.
- [8] A. Blake, Boundary conditions for lightness computation in Mondrian world, *Comput. Vis. Graph. Image Process.* 32 (3) (1985) 314–327.
- [9] A.B. Petro, Fast implementation of color constancy algorithms, *Proce. SPIE Int. Soc. Opt. Eng.* 7241 (2009) 724106.
- [10] J.M. Morel, A.B. Petro, C. Sbert, A PDE formalization of Retinex theory, *IEEE Trans. Image Process.* 19 (11) (2010) 2825–2837.
- [11] W.-Y. Ma, S. Osher, A tv bregman iterative model of retinex theory, *Inverse Probl. Imag.* 6 (4) (2012) 697–708.
- [12] M.K. Ng, W. Wang, A total variation model for retinex, *SIAM J. Imag. Sci.* 4 (1) (2011) 345–365.
- [13] W. Wang, C.-J. He, A variational model with barrier functionals for retinex, *SIAM J. Imag. Sci.* 8 (3) (2015) 1955–1980.
- [14] X.-Y. Fu, D.-L. Zeng, Y. Huang, X.-P. Zhang, X.-H. Ding, A weighted variational model for simultaneous reflectance and illumination estimation, in: *Proceedings of the IEEE Conference on Computer Vision and Pattern Recognition*, 2016, pp. 2782–2790.
- [15] D. Zosso, G. Tran, S.J. Osher, Non-local retinex—a unifying framework and beyond, *SIAM J. Imag. Sci.* 8 (2) (2015) 787–826.
- [16] W. Wang, M.K. Ng, A nonlocal total variation model for image decomposition: Illumination and reflectance., *Numer. Math. Theory Meth. Appl.* 7 (3) (2014) 334–355.
- [17] W. Ma, J.-M. Morel, S. Osher, A. Chien, An L1-based variational model for Retinex theory and its application to medical images, in: *Proceedings of the IEEE Conference on Computer Vision and Pattern Recognition*, 2011, pp. 153–160.
- [18] H.-F. Li, L.-P. Zhang, H.-F. Shen, A perceptually inspired variational method for the uneven intensity correction of remote sensing images, *IEEE Trans. Geosci. Remote Sens.* 50 (8) (2012) 3053–3065.
- [19] H.-B. Chang, M.K. Ng, W. Wang, T.-Y. Zeng, Retinex image enhancement via a learned dictionary, *Opt. Eng.* 54 (1) (2015) 013107.
- [20] R. Kimmel, M. Elad, D. Shaked, R. Keshet, I. Sobel, A variational framework for Retinex, *Inter. J. Comput. Vis.* 52 (1) (2003) 7–23.
- [21] J.-W. Liang, X.-Q. Zhang, Retinex by higher order total variation L^1 decomposition, *J. Math. Imag. Vis.* 52 (3) (2015) 345–355.
- [22] T.-H. Ma, Y. Lou, T.-Z. Huang, Truncated L1-2 models for sparse recovery and rank minimization, *SIAM J. Image Sci.* (2017).
- [23] J. Huang, D. Mumford, Statistics of natural images and models, in: *Proceedings of the IEEE Conference on Computer Vision and Pattern Recognition*, 1999, pp. 541–547.
- [24] D.L. Ruderman, The statistics of natural images, *Netw. Comput. Neural Syst.* 5 (4) (1994) 517–548.
- [25] D. Field, What is the goal of sensory coding? *Neural Comput.* 6 (4) (1994) 559–601.
- [26] A. Levin, R. Fergus, F. Durand, W. Freeman, Image and depth from a conventional camera with a coded aperture, *AcM Trans. Graph.* 26 (3) (2007) 70.
- [27] E.P. Simoncelli, E.H. Adelson, Noise removal via Bayesian wavelet coring, in: *Proceedings of the International Conference on Image Processing*, 1, 1996, pp. 379–382.
- [28] D. Krishnan, R. Fergus, Fast image deconvolution using hyper-laplacian priors, in: *Advances in Neural Information Processing Systems*, 2009, pp. 1033–1041.
- [29] W.-M. Zuo, D.-W. Ren, S.-H. Gu, L. Lin, L. Zhang, Discriminative learning of iteration-wise priors for blind deconvolution, in: *Proceedings of the IEEE Conference on Computer Vision and Pattern Recognition*, 2015, pp. 3232–3240.
- [30] Y. Chang, L.-X. Yan, S. Zhong, Hyper-laplacian regularized unidirectional low-rank tensor recovery for multispectral image denoising, in: *Proceedings of the IEEE Conference on Computer Vision and Pattern Recognition*, 2017, pp. 5901–5909.
- [31] J.-J. Mei, Y.-Q. Dong, T.-Z. Huang, W.-T. Yin, Cauchy noise removal by nonconvex admm with convergence guarantees, *J. Sci. Comput.* 74 (2) (2018) 1–24.
- [32] T.-Y. Ji, T.-Z. Huang, X.-L. Zhao, T.-H. Ma, L.-J. Deng, A non-convex tensor rank approximation for tensor completion, *Appl. Math. Model.* 48 (2017) 410–422.
- [33] S. Boyd, N. Parikh, E. Chu, B. Peleato, Distributed optimization and statistical learning via the alternating direction method of multipliers, *Trends Mach. Learn.* 3 (1) (2010) 1–122.
- [34] X.-L. Zhao, F. Wang, M.K. Ng, A new convex optimization model for multiplicative noise and blur removal, *SIAM J. Image Sci.* 7 (1) (2014) 456–475.
- [35] A. Nedic, D.P. Bertsekas, A.E. Ozdaglar, *Convex Analysis and Optimization*, Athena Scientific, 2003.
- [36] X.-L. Zhao, F. Wang, T.-Z. Huang, M.K. Ng, R.J. Plemmons, Deblurring and sparse unmixing for hyperspectral images, *IEEE Trans. Geosci. Remote Sens.* 51 (7) (2013) 4045–4058.
- [37] J. Huang, M. Donatelli, R.H. Chan, Nonstationary iterated thresholding algorithms for image deblurring, *Inverse Probl. Imaging* 7 (3) (2013) 717–736.
- [38] Y. Chen, T.-Z. Huang, L.-J. Deng, X.-L. Zhao, M. Wang, Group sparsity based regularization model for remote sensing image stripe noise removal, *Neurocomputing* (2017).
- [39] M.K. Ng, P. Weiss, X.-M. Yuan, Solving constrained total-variation image restoration and reconstruction problems via alternating direction methods, *SIAM J. Image Sci.* 32 (5) (2010) 2710–2736.
- [40] W.-M. Zuo, D.-Y. Meng, L. Zhang, X.-C. Feng, D. Zhang, A generalized iterated shrinkage algorithm for non-convex sparse coding, in: *Proceedings of the IEEE international conference on computer vision*, 2013, pp. 217–224.

- [41] S.-H. Wang, J. Zheng, H.-M. Hu, B. Li, Naturalness preserved enhancement algorithm for non-uniform illumination images, *IEEE Trans. Image Process.* 22 (9) (2013) 3538–3548.
- [42] A. Mittal, R. Soundararajan, A.C. Bovik, Making a completely blind image quality analyzer, *IEEE Signal Process. Lett.* 20 (3) (2013) 209–212.
- [43] S.-H. Chen, A. Beghdadi, Natural rendering of color image based on retinex, in: Proceedings of the 2009 16th IEEE International Conference on Image Processing (ICIP), IEEE, 2009, pp. 1813–1816.
- [44] H. Attouch, J. Bolte, P. Redont, A. Soubeyran, Proximal alternating minimization and projection methods for nonconvex problems: An approach based on the Kurdyka–Łojasiewicz inequality, *Math. Oper. Res.* 35 (2) (2010) 438–457.
- [45] A. Ben-Tal, M. Teboulle, Hidden convexity in some nonconvex quadratically constrained quadratic programming, *Math. Progr.* 72 (1) (1996) 51–63.